SANDIA REPORT

SAND2013-8812
Unlimited Release
Printed October 2013

Development of Ab Initio Techniques Critical for Future Science-Based Explosives R&D.

Ryan R. Wixom and Ann E. Mattsson

Prepared by
Sandia National Laboratories
Albuquerque, New Mexico 87185 and Livermore, California 94550

Sandia National Laboratories is a multi-program laboratory managed and operated by Sandia Corporation, a wholly owned subsidiary of Lockheed Martin Corporation, for the U.S. Department of Energy's National Nuclear Security Administration under contract DE-AC04-94AL85000.

Approved for public release; further dissemination unlimited.

Sandia National Laboratories

Issued by Sandia National Laboratories, operated for the United States Department of Energy by Sandia Corporation.

NOTICE: This report was prepared as an account of work sponsored by an agency of the United States Government. Neither the United States Government, nor any agency thereof, nor any of their employees, nor any of their contractors, subcontractors, or their employees, make any warranty, express or implied, or assume any legal liability or responsibility for the accuracy, completeness, or usefulness of any information, apparatus, product, or process disclosed, or represent that its use would not infringe privately owned rights. Reference herein to any specific commercial product, process, or service by trade name, trademark, manufacturer, or otherwise, does not necessarily constitute or imply its endorsement, recommendation, or favoring by the United States Government, any agency thereof, or any of their contractors or subcontractors. The views and opinions expressed herein do not necessarily state or reflect those of the United States Government, any agency thereof, or any of their contractors.

Printed in the United States of America. This report has been reproduced directly from the best available copy.

Available to DOE and DOE contractors from
U.S. Department of Energy
Office of Scientific and Technical Information
P.O. Box 62
Oak Ridge, TN 37831

Telephone: (865) 576-8401
Facsimile: (865) 576-5728
E-Mail: reports@adonis.osti.gov
Online ordering: http://www.osti.gov/bridge

Available to the public from
U.S. Department of Commerce
National Technical Information Service
5285 Port Royal Rd
Springfield, VA 22161

Telephone: (800) 553-6847
Facsimile: (703) 605-6900
E-Mail: orders@ntis.fedworld.gov
Online ordering: http://www.ntis.gov/help/ordermethods.asp?loc=7-4-0#online

SAND2013-8812
Unlimited Release
Printed October 2013

Development of Ab Initio Techniques Critical for Future Science-Based Explosives R&D.

Ryan R. Wixom
EM Dynamic and Reactive Sciences, 2554
Sandia National Laboratories
P.O. Box 5800
Albuquerque, NM 87185-1454
rrwixom@sandia.gov

Ann E. Mattsson
Computational Shock and Multiphysics MS 1322
Sandia National Laboratories
P.O. Box 5800
Albuquerque, NM 87185-1322
aematts@sandia.gov

Abstract

Density Functional Theory (DFT) has emerged as an indispensable tool in materials research, since it can accurately predict properties of a wide variety of materials at both equilibrium and extreme conditions. However, for organic molecular crystal explosives, successful application of DFT has largely failed due to the inability of current exchange-correlation functionals to correctly describe intermolecular van der Waals' (vdWs) forces. Despite this, we have discovered that even with no treatment of vdWs bonding, the AM05 functional and DFT based molecular dynamics (MD) could be used to study the properties of molecular crystals under compression. We have used DFT-MD to predict the unreacted Hugoniots for PETN and HNS and validated the results by comparison with crystalline and porous experimental

data. Since we are also interested in applying DFT methods to study the equilibrium volume properties of explosives, we studied the nature of the vdWs bonding in pursuit of creating a new DFT functional capable of accurately describing equilibrium bonding of molecular crystals. In this report we discuss our results for computing shock Hugoniots of molecular crystals and also what was learned about the nature of bonding in these materials.

Acknowledgment

The authors would like to thank Thomas Mattsson, David Damm, Kyle Cochrane, George Cragg, and Anatole von Lilienfeld for their contributions and assistance.

Sandia National Laboratories is a multi-program laboratory managed and operated by Sandia Corporation, a wholly owned subsidiary of Lockheed Martin Corporation, for the U.S. Department of Energy's National Nuclear Security Administration under contract DE-AC04-94AL85000.

Contents

Nomenclature **11**

1 Introduction and Motivation **13**

2 Density Functional Theory **15**

3 Shock Properties of Molecular Crystal Explosives **17**

Method 17

Results: Pentaerythritol Tetranitrate (PETN) 18

Results: Hexanitrostilbene (HNS) 21

Toward a Tabular Equation of State 22

4 The origins of van der Waals' forces **23**

The two-hydrogen system 23

Perturbation theory 23

Unperturbed single electron system 24

Unperturbed two electron system 25

The perturbation 25

First order perturbation theory 26

Energy 27

Wave functions 27

Second order perturbation theory 30

Summary 31

5 Density Functional Theory exchange-correlation functionals **33**

$1/R^6$ functionals 33

Non-local functionals 34

6 Summary and Conclusion **35**

References **36**

List of Figures

1.1 The foundation of Science Based Engineering is to build bridges from the fundamental Laws of Nature up to the Engineering codes, bridging several length and time scales. In this figure two different paths are depicted. The upper one is quite complicated and illustrates the general problem of bridging several different scales. The lower path is already in use at Sandia. For Equation of State construction, data provided by Density Functional Theory (DFT) based calculations are used in addition to experimental data. The DFT calculations are used in two ways, either directly or as a provider of forces in a Molecular Dynamics scheme. 14

2.1 The exact functional would give the exact density, ρ, and thus the exact properties via density functionals, $F[\rho]$. The unknown wave function density functional, $\Psi[\rho]$, would in this case give all properties that can be calculated from the Schrödinger equation exactly. However, the mean field view of using the KS orbitals as approximate electron wave functions would be approximate. Only the density and properties calculated via density functionals are guaranteed to be exact. The quality of a functional can thus not be judged by how well it reproduces wave function derived properties. From Reference 15. 16

3.1 The unreacted Hugoniot of PETN shown in both pressure-volume and velocity space. Red points are computed via DFT-MD. Open circles are single-crystal data from the LASL shock handbook.[16] The red-dashed line is a quadratic fit to the DFT data and the black line is a linear extrapolation of the experimental data. 19

3.2 Transformation of the crystalline Hugoniot of PETN to that of two lower densities, chosen to match available experimental data.[22,23] 21

3.3 DFT-MD predicted Hugoniot of HNS at TMD (solid line) and experimental data at 1.7 g/cc (red circles), 1.6 g/cc (blue triangles), 1.0 g/cc (green squares). Dashed lines are porous transformation of the crystalline prediction for densities matching the experiments. 22

4.1 The external potential for a two hydrogen system (black). The individual hydrogen potentials are gray dashed and the electrons are predominantly moving in the shaded blue areas. Note the classically forbidden region between the individual hydrogen atoms; only electrons with very high kinetic energy can penetrate this region but it is also these electrons that have any chance of knowing about the other half of the system. 24

4.2 The states, here illustrated by the $2p_z$ states, on each atom, are well localized and do not overlap. 30

5.1 A Lennard-Jones 6-12 potential approximately describing the the binding energy of two Ar atoms at distance r. As is seen, the $1/r^6$ term diverges as the distance between the atoms is decreasing and a damping term is needed to turn the potential upwards for correct binding profile. 34

Nomenclature

Dirac The Dirac Equation: The relativistic quantum mechanical wave equation describing electrons in relativistic matter, such as heavy materials like actinides.

SE The Schrödinger Equation: The non-relativistic limit of the Dirac Equation, sufficiently accurate to describe electrons in lighter materials.

DFT Density Functional Theory: The formally exact reformulation of the wave-function based Schrödinger and Dirac Equations in terms of density and currents.

KS The Kohn-Sham Equations: A calculational approach derived from the Dirac/SE using DFT. These are the equations implemented in DFT codes.

Functional A short name for an approximation for the Exchange-Correlation functional which is the only part of DFT that needs to be approximated. The functional sets the possible accuracy of DFT calculations.

LMTO Linear Muffin Tin Orbital: A calculational method used in the RSPt code.

LAPW Linear Augmented Plane Wave: Another calculational method. It is considered the implementation method that gives the most accurate DFT results. Other methods are usually verified against this method.

plane-wave code A code using plane waves as a basis set. This is the computationally most effective approach because Fourier Transforms can be used. Calculations can also be systematically improved by increasing the number of basis functions used, usually specified by the so called 'cut-off'. However, describing core electrons accurately requires a very large cut-off, leading to expensive calculations. The plane-wave approach thus is mostly used together with pseudo-potentials (see below).

all-electron code A code treating all electrons explicitly. LMTO and LAPW codes are all-electron.

pseudo-potential code The chemically inert core electrons are treated in a collective way via pseudo potentials, which increases the computational efficiency considerably. A number of different approaches exist; all are verified by comparing to all-electron, usually LAPW, results.

PAW Projected Augmented Wave: The pseudo potential technique currently considered the most accurate.

RSPt Relativistic Spin-Polarised test: The name of an all-electron, full potential, LMTO code developed by Dr. John M. Wills at Los Alamos National Laboratory.

VASP Vienna *Ab-initio* Simulation Package: A plane wave, pseudo potential (PAW), DFT code extensively used at Sandia.

core electron An electron close to the nucleus. In an LMTO or LAPW treatment these electrons are considered inert and their properties only depend on the closest nuclei. In a pseudo-potential code the effect of the core electrons on the valence electrons is included via pseudo potentials.

semi-core electron An electron that is intermediate between a core and a valence electron. It has the same angular momentum quantum number as some of the valence electrons but has a lower principal quantum number (it is in a lower shell). For the heavier nuclei (or for lighter nuclei at high pressure) these electrons need to be treated as valence electrons.

valence electron The outermost electrons are valence electrons and their properties are dependent on many nuclei. These electrons are forming bonds that hold a solid or molecule together.

Chapter 1

Introduction and Motivation

Density functional theory (DFT) is the preferred computational method for exploring materials properties, and Sandia scientists are at the forefront of DFT-based equation of state (EOS) construction, where information from both experiments and computational investigations are used (See Figure 1.1). DFT[8,10] is a formally exact reformulation of the Schrödinger Equation (SE) for the ground state of an electron system. Since the DFT equations are far easier to solve than the many-body SE, DFT has become the preferred computational method for exploring properties of materials. One example of a Sandia effort in this area is the recent use of DFT results combined with Z experiments to construct a new Quartz standard leading to resolution of an important discrepancy between flyer plate and laser driven shock data for deuterium.[9] Another example is similar work for Xenon,[21] a material of importance for DOE. Here DFT results helped both in showing that the available Equation of State (EOS) tables were inaccurate at high pressures and in the construction of a new, more accurate, EOS.

Accurate equation of state data for energetic materials is scarce, despite many decades of experimental effort. Yet, this data is critical for building predictive simulations of energetic component performance. Motivated by the work noted above on, we have explored the use of DFT methods for predicting the shock properties of molecular crystal explosives. It is well-known that DFT does not accurately describe the dispersion forces that bind the equilibrium structure of molecular crystals. This problem has discouraged the use of DFT for studying the properties of many explosives. However, since our main interest is the response of explosives under high pressure (shock) loading, we correctly hypothesized that for this special case small errors in the intermolecular attractive forces could be neglected. In this report we describe how DFT based molecular dynamics (MD) were applied to predict the shock Hugoniots of PETN and HNS. We also discuss the limitations of this approach and the remaining questions associated with DFT and van der Waals' forces.

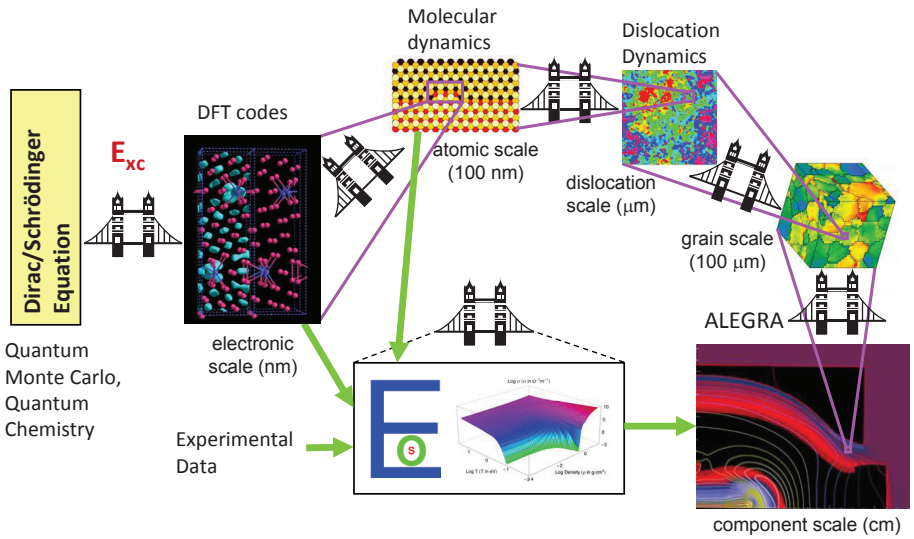

Figure 1.1. The foundation of Science Based Engineering is to build bridges from the fundamental Laws of Nature up to the Engineering codes, bridging several length and time scales. In this figure two different paths are depicted. The upper one is quite complicated and illustrates the general problem of bridging several different scales. The lower path is already in use at Sandia. For Equation of State construction, data provided by Density Functional Theory (DFT) based calculations are used in addition to experimental data. The DFT calculations are used in two ways, either directly or as a provider of forces in a Molecular Dynamics scheme.

Chapter 2

Density Functional Theory

Density Functional Theory (DFT) is an exact reformulation of the fundamental law of nature governing the behavior of electrons. If electrons are in materials with heavy ions, the fundamental law is the Dirac equation. For materials composed of lighter ions, the non-relativistic limit of the Dirac equation, the Schrödinger equation, might be used.

Density Functional Theory was first developed using the Schrödinger equation. Using the Hohenberg-Kohn theorem,[8] the Schrödinger equation, which decides the electronic properties of a material via many-body electronic wave-functions, can be cast in the form of the Kohn-Sham (KS) equations, which instead decide the behavior of ground state electrons via auxiliary non-interacting single particle Kohn-Sham orbitals forming the true electron density of the material. The key point is that solving for non-interacting single particles is a much less demanding task than solving for many-body wave-functions.

Despite the theory in itself being exact, approximations for the *Exchange-Correlation functional* still need to be done since the form of this object is unknown. The accuracy of the approximation for the Exchange-Correlation functional is the factor that decides the ultimately attainable accuracy of the calculations. No calculations based on DFT can ever give better results than this approximation allows. If the 'divine'[17] functional were known, however, the KS equations would yield the exact same results as the fundamental law of nature, the Schrödinger Equation.

The KS equations are often interpreted as the equations of electrons moving in a field formed by all the other electrons, so called mean-field theory. From a mean-field theory perspective the KS orbitals can be interpreted as approximations for the true many-body electron wave-functions. This alternative interpretation of the KS equations can be very fruitful if handled correctly, but it also has created, and is creating, a lot of confusion in the field. In Figure 2.1 we try to compare the two views. In addition to the 'pure' KS equations, several mean-field theory based schemes are also implemented in VASP.

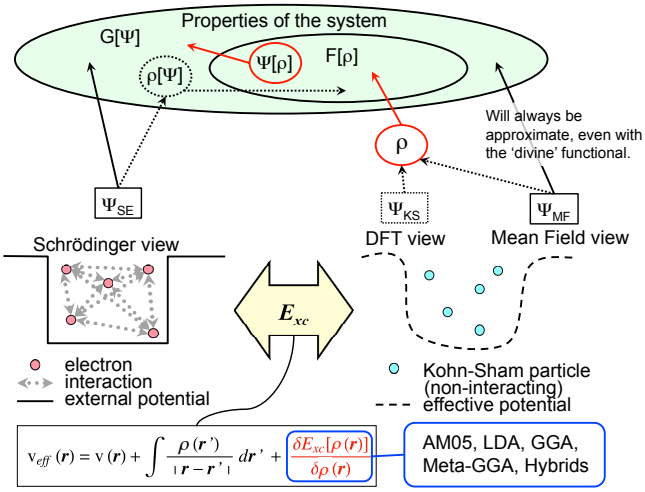

Figure 2.1. The exact functional would give the exact density, ρ, and thus the exact properties via density functionals, $F[\rho]$. The unknown wave function density functional, $\Psi[\rho]$, would in this case give all properties that can be calculated from the Schrödinger equation exactly. However, the mean field view of using the KS orbitals as approximate electron wave functions would be approximate. Only the density and properties calculated via density functionals are guaranteed to be exact. The quality of a functional can thus not be judged by how well it reproduces wave function derived properties. From Reference 15.

Chapter 3

Shock Properties of Molecular Crystal Explosives

Method

The equilibrium volume inter-molecular physics of PETN and other CHNO molecular crystal explosives are dominated by van der Waals' (vdWs') forces. No currently available exchange-correlation functional correctly treats vdWs' forces, which is likely the main reason that application of DFT to energetic molecular crystals hasn't been very successful. The other available ab-initio exchange-correlation functionals (e.g. LDA, PBE) have some amount of spurious vdWs' like binding. It has been proposed[2,18] that under strong compression, inaccurate treatment of the weak attractive forces should become less and less significant. We feel that for the research presented here, AM05 is particularly suited due to its unique character of not including any vdWs' attraction. That is, the lack of treatment is more tolerable than incorrect treatment. As such, we expect that near equilibrium, there is some error associated with the lack of vdWs' attraction, but under some level of compression the error will become irrelevant and the technique will provide accurate results for studying material response under strong compression.

Unreacted principle Hugoniots were predicted from first-principles using density functional theory based molecular dynamics (DFT-MD). Our calculations, utilizing the AM05[1] functional, were performed with the Vienna ab-initio simulation package (VASP 5.2),[11–13] using strictly converged settings.[19] The plane-wave cut-off was set to 800 eV and k-point sampling with mean-value point (1/4,1/4,1/4) was used. The ionic time-step was set to 0.4 fs. Because DFT doesn't accurately describe the equilibrium structure of molecular crystals, the reference state was taken to be the experimental structure and volume of each material studied. For PETN,[4] the tetragonal reference state lattice parameters were taken to be $a = 0.93776$ and $c = 0.67075$.For HNS,[6] the monoclinic $P21/c$ reference state lattice parameters were taken to be $a = 22.326$, $b = 5.5706$, $c = 14.667$, and $\beta = 110.04°$.

Points along the Hugoniot were found by setting the volume ($V < V_0$) and equilibrating by running an NVT simulation (Nose-Hoover thermostat) for up to six picoseconds. The temperature of that cell was then instantly increased in three separate trajectories, which continued for an additional six picoseconds. The pressure and energy from equilibrated portions of these runs were then used to write equations $U(T)$ and $P(T)$. These equations,

and the conservation of energy Rankine-Hugoniot relation, $[U(T)-U_0] = 1/2[P(T)+P_0][V_0-V]$, were then used to solve for the temperature on the Hugoniot. That temperature is then used to determine the pressure and energy on the Hugoniot for that set volume. Repeating this with increasing densities allows one to map out the unreacted Hugoniot to very high pressures, much higher than is achievable experimentally. This method provides everything that is needed to write a complete equation of state (P, V, T, E).

Results: Pentaerythritol Tetranitrate (PETN)

Figure 3.1 shows the DFT-MD predicted unreacted crystalline principle Hugoniot of PETN and compares it to experimental data from the LASL shock handbook.[16] The velocity plot in Fig 3.1 illustrates a major weakness in experimentally determined shock data for explosives, that the data is only available for relatively low shock velocities. It is difficult to make measurements at higher impact velocities due to the reactive nature of the material. Unfortunately, higher pressure data is critical for building predictive simulations since the material in front of a detonation wave is first shocked to a point on the unreacted Hugoniot before it has time to react. The solid line in the plot is the Hugoniot obtained from extrapolating the experimental data. It clearly doesn't capture the high pressure curvature predicted by theory, nor the low pressure curvature evident from experiment, and the resulting discrepancy in pressure may be as much as 10%. There is no reason to believe that the $U_s u_p$ relationship of any material should follow a polynomial of any order. Clearly a line is inadequate, and a second order polynomial fit to the PETN data has an inflection before reaching detonation pressure. This is not an indictment of empirical shock data, but a comment about the danger of extrapolating EoS data wether it is obtained via theory or experiment.

It is important to note that the described DFT-MD method provides the Hugoniot of the the perfect crystal, often referred to as the crystalline Hugoniot. Almost all available shock data for explosives is measured for consolidated powders with densities less than the crystalline density. However, with a few fairly reasonable assumptions, it is possible to transform the crystalline Hugoniot to that of any density.

When transforming the crystalline Hugoniot to shock compression of the porous material, the first assumption is that the stress required to completely crush the pores is negligible (i.e. the initially porous material becomes completely compacted at negligible stress). We will use the Rankine-Hugoniot relations for mass, momentum and energy conservation across a shock jump.

$$vU_s = v_0(U_s - u_p) \tag{3.1}$$

$$Pv_0 = u_p U_s \tag{3.2}$$

$$e - e_0 = \frac{1}{2}P(v_0 - v) \tag{3.3}$$

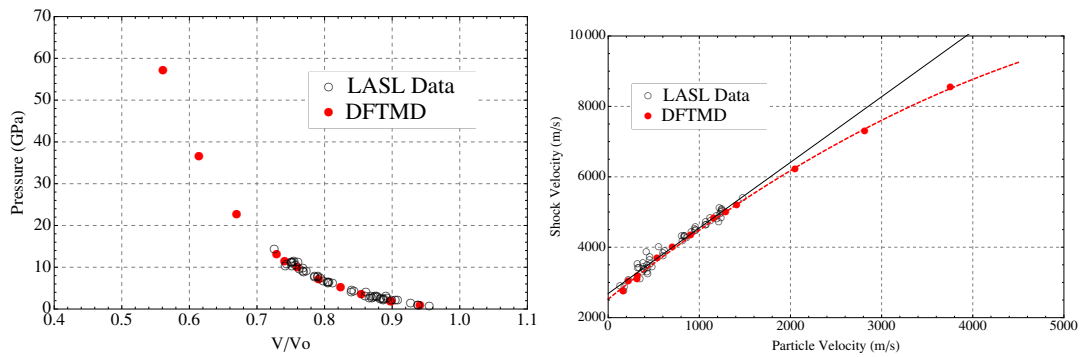

Figure 3.1. The unreacted Hugoniot of PETN shown in both pressure-volume and velocity space. Red points are computed via DFT-MD. Open circles are single-crystal data from the LASL shock handbook.[16] The red-dashed line is a quadratic fit to the DFT data and the black line is a linear extrapolation of the experimental data.

If appropriate, the initial pressure and particle velocity can be assumed zero, v_0 is the initial specific volume, v is the equilibrium volume behind the shock front, U_s is the shock velocity, u_p is the particle velocity, P is the equilibrium pressure behind the shock front (assume pressure and stress are equal), and e is the internal energy of the material.

The relationship between shock velocity and particle velocity is a material property that, for lack of a better option, is often expressed as a polynomial,

$$U_s = C_0 + S_1 u_p + S_2 u_p^2 \tag{3.4}$$

where C_0, S_1, and S_2 are constants which, in our case, have been fit to the DFT-MD predicted crystalline Hugoniot. In order to find the Hugoniot of the porous material, recall the definition of the Gruneisen parameter,

$$\Gamma = v\frac{(P - P_0)}{(e - e_0)}. \tag{3.5}$$

Next we assume that the solid material and the porous material have the same reference state,[5] $P_0 = P_0^*$ and $e_0 = e_0^*$. This condition is exactly satisfied on the 0 K isotherm,[24] however Erkman[5] simplified the approach greatly by using the Hugoniot of the solid as the reference state. It follows from 3.5, that the pressure-energy state relationships for the solid and porous materials are,

$$P = \frac{\Gamma}{v}(e - e_0) \qquad \text{(solid)} \tag{3.6}$$

and

$$P^* = \frac{\Gamma}{v}(e^* - e_0) \qquad \text{(porous*)}. \tag{3.7}$$

When these two equations are combined the pressure in the porous material can be related to the pressure in the solid (fully-dense) material at any desired shock jump condition, v, as

$$P - P^* = \frac{\Gamma}{v}(e - e^*). \tag{3.8}$$

We now substitute equation 3.3 for both the solid and porous materials into equation 3.8 to obtain

$$P - P^* = \frac{\Gamma}{v}\left(\frac{1}{2}P(v_0 - v) - \frac{1}{2}P^*(v_0^* - v)\right), \tag{3.9}$$

which can be rearranged and solved for the pressure in the porous material,

$$P^* = P\frac{v_0 - v - \frac{2v}{\Gamma}}{v_0^* - v - \frac{2v}{\Gamma}}. \tag{3.10}$$

Solving equation 3.1 for particle velocity in the porous material, u_p^*, yields

$$u_p^* = \frac{U_s^*(v_0^* - v)}{v_0^*}. \tag{3.11}$$

The shock velocity in the porous martial, U_s^*, is then found by substituting equation 3.11 into equation 3.2 and then solving for the shock velocity,

$$U_s^* = v_0^*\sqrt{\frac{P^*}{(v_0^* - v)}}. \tag{3.12}$$

Using these last three equations, the pressure, shock velocity, and particle velocity in the porous material may be found for any given compressed volume.

Notice that this result does not depend on the microstructure of the porous material (grain size, morphology, pore size, specific surface area, etc.); it only depends on the initial density. This derivation is only valid in the regime of stress levels which are much higher than what is required for compaction. When stress levels required for compaction are not negligible, then a constitutive compaction model such as proposed by Herrmann[7] or Carroll and Holt[3] is required. The constitutive compaction model in general will depend strongly on the details of the microstructure and the strength of the solid material.

Figure 3.2 shows the unreacted Hugoniot of PETN at three different densities: theoretical maximum density (1.74 g/cc), 1.7 g/cc, and 1.0 g/cc. The theoretical maximum density (TMD) line is a quadratic fit to the DFT-MD data shown previously, and is included here for reference. The limited low pressure unreacted data at 1.7 and 1.0 g/cc were taken from the literature.[22,23] Considering the assumptions being made, the agreement is excellent and provides a second confirmation that the pressure and density states computed via DFT-MD are extremely accurate. In the second plot of Figure 3.2 the 1.0 g/cc data illustrates the need for including a compaction model for low density and pressure conditions, but such a model is out of the scope of this work.

The success of applying this method to PETN, where there is crystalline data for validation, provided the confidence to use this method for other explosives where data doesn't exist. After all, the true value of DFT methods in general is for computing material properties when empirical data is not available.

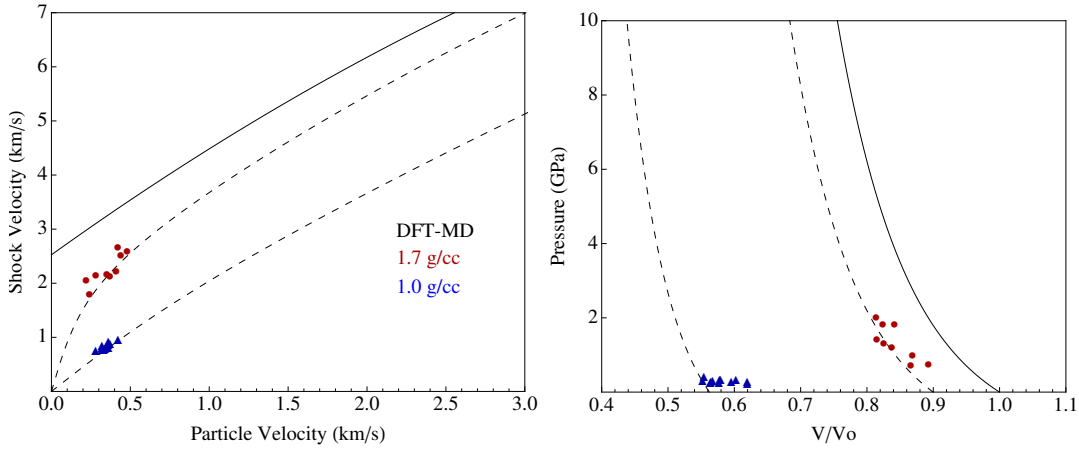

Figure 3.2. Transformation of the crystalline Hugoniot of PETN to that of two lower densities, chosen to match available experimental data.[22,23]

Results: Hexanitrostilbene (HNS)

The relatively insensitive and temperature tolerant explosive HNS is technological significant to the NW stockpile, and is found in several Sandia components. In order to facilitate predictive simulation of component performance, an accurate EoS for HNS is needed. Like many other secondary explosives, no crystalline shock data has been collected for HNS. Several researchers have measured the $U_s u_p$ relationship for porous HNS at low pressures, but the scatter in the empirical data and the limited range of shock pressures and initial densities leads to unacceptable uncertainty in an empirically generated EoS for HNS.

The method described above was applied to HNS. The results are shown in Figure 3.3, represented as both the pressure-volume and $U_s u_p$ relationship. Since there is no crystalline data, the DFT-MD crystalline Hugoniot is truly a prediction. However, by transforming the crystalline relationship to lower density, using the previously described method, we can indirectly validate our EoS by comparison with porous experimental data. As with PETN, the agreement is excellent. Furthermore, considering the scatter in the data, it is evident that these relationships would be extremely difficult to generate by fitting a line to the empirical data. At this point is seems prudent to compute the relationships using our method and then use a few well chosen experiments for validation. That approach will lead to more accurate EoSs and be more financially tenable.

Since many people performing simple hydrocode simulations will use a Mie-Gruneisen EoS, we have fit a quadratic to the DFT-MD predicted Hugoniot, $2755 + 1.871x - 1.152 \times 10^{-4}x^2(m/s)$. At this time we make no recommendation as to the appropriate values of C_v and Γ. For use in CTH the user defined values, for $1.745g/cc$ HNS, are $C_0 = 2.755 \times 10^5(cm/s)$, $S_1 = 1.871$, and $S_2 = -0.317$.

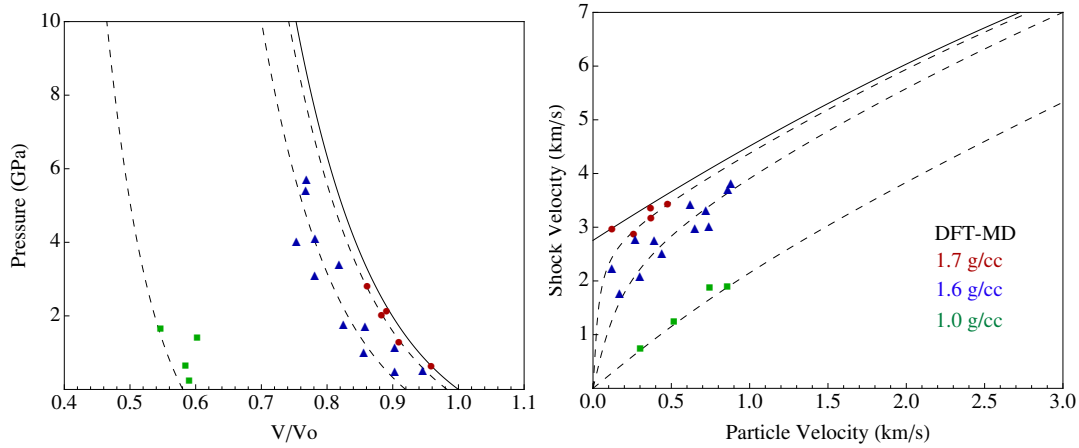

Figure 3.3. DFT-MD predicted Hugoniot of HNS at TMD (solid line) and experimental data at 1.7 g/cc (red circles), 1.6 g/cc (blue triangles), 1.0 g/cc (green squares). Dashed lines are porous transformation of the crystalline prediction for densities matching the experiments.

Toward a Tabular Equation of State

We previously stated that the described method provides all of the information necessary to predict a complete equation of state. However, temperature and internal energy are not easily measured, especially under the temporal time constraints of shocked explosives. Future work will involve a thorough examination of the DFT-MD predicted temperature, internal energy, and other thermo-physical properties derived from them. We are also hopeful that new ultra-fast spectroscopic measurements will provide future data for validation. While we have created a tabular equation of state (for use in CTH) from the predicted HNS shock properties, it is currently being tested and not ready for distribution. A future publication will detail and demonstrate a tabular EoS that will be made widely available.

Chapter 4

The origins of van der Waals' forces

Van der Waals' forces are very weak. In most systems they are negligible compared to stronger forces and only in a few types of systems do they dominate the physics. One such type of system is noble gases, composed of elements like helium, neon, or argon, which all are found in the rightmost column in the periodic table. Noble gases have atoms with all shells closed, that is, the number of electrons are exactly such that they can pair up in a very efficient way, forming very stable and inert neutral atoms.

Another type of systems, of particular interest for this project, are molecular crystals. In these crystals, fairly inert molecules are held together in a periodic structure by the weak van der Waals' forces. However, while this picture is correct at equilibrium, it is not an appropriate description when the molecular crystal is either heated up or put under pressure (or both). Under pressure the molecules are forced together to distances that promote interaction either between the molecules or within a distorted molecule. Heat increases the internal motion of the atoms in the molecules and make them less inert. Loosely speaking the van der Waals' forces are of importance for the safety of a molecular crystal explosive, while the internal energy stored in the bonds of the molecules are important for the action of the explosive. Understanding van der Waals' forces are thus mainly important for questions related to aging and safety.

The two-hydrogen system

While a hydrogen atom is not a noble gas atom, we can study the importance of electrons in one part of a system interacting with electrons on another, distant, part. The system we are investigating is depicted in Figure 4.1. Note the classically forbidden region between the two systems; we will keep $\boldsymbol{R}$ large enough to always have such a region in the system.

Perturbation theory

As is seen in Figure 4.1 the electrons in the two systems (mostly remaining in the blue shaded areas) at a large distance $\boldsymbol{R}$, are virtually unperturbed from their atomic configuration (blue shaded area in one system with external potential as the gray dashed line).

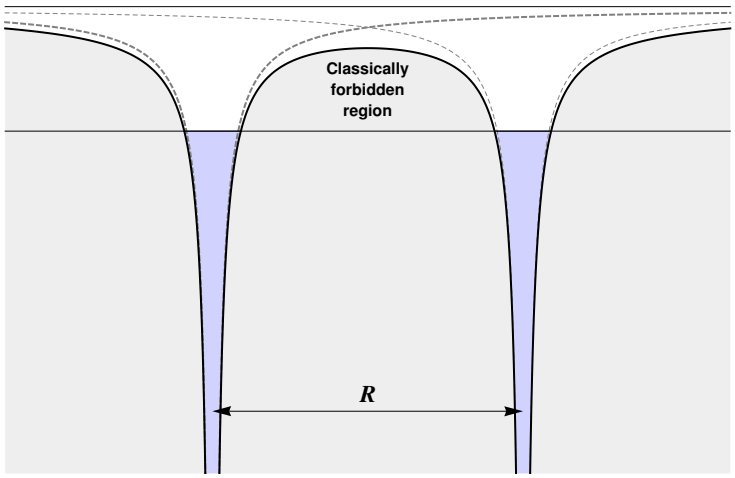

Figure 4.1. The external potential for a two hydrogen system (black). The individual hydrogen potentials are gray dashed and the electrons are predominantly moving in the shaded blue areas. Note the classically forbidden region between the individual hydrogen atoms; only electrons with very high kinetic energy can penetrate this region but it is also these electrons that have any chance of knowing about the other half of the system.

Perturbation theory on the unperturbed atoms is thus expected to work well.

Unperturbed single electron system

The system of a single electron moving in a coulombic $-Z/\boldsymbol{r}$ potential (Z is the nuclear charge or the atomic number), such as the gray dashed one in Figure 4.1, is exactly solvable analytically. The single electron wave functions are

$$\psi_{nLM}(r,\theta,\phi) = \left[\left(\frac{2Z}{n}\right)^3 \frac{(n-L-1)!}{2n(n+L)!}\right]^{\frac{1}{2}} e^{-\frac{Zr}{n}} \left(\frac{2Zr}{n}\right)^L L_{n-L-1}^{2L+1}(\frac{2Zr}{n})\, Y_L^M(\theta,\phi)\,, \tag{4.1}$$

where $\boldsymbol{r} = (r,\theta,\phi)$ and the integers $n = 1, 2, \cdots,\ L = 0, \cdots, n-1$, and $M = -L, \cdots, L$. L_n^m is a generalized Laguerre polynomial and Y_L^M is a spherical harmonic. The energy of the unperturbed system is

$$E_n = -\frac{Z^2}{n^2} Ry\,, \tag{4.2}$$

where Ry is the Rydberg energy unit.

Unperturbed two electron system

A two electron system should be described by fermionic two-body wave functions:

$$\Psi_{\text{elec}}(\boldsymbol{r}_1, \boldsymbol{r}_2) = \psi_1(\boldsymbol{r}_1)\psi_2(\boldsymbol{r}_2) - \psi_1(\boldsymbol{r}_2)\psi_2(\boldsymbol{r}_1)\,. \tag{4.3}$$

A fermionic wave function should transform into the negative of itself when trading the positions of the two electrons.

If we restrict ourselves to the hydrogen ($Z = 1$) $1s$-states, that is, $n = 1$, $L = 0$, and $M = 0$, we have

$$\psi_1(\boldsymbol{r}) = \frac{1}{\sqrt{\pi}} e^{-|\boldsymbol{r}|}\,, \text{and} \quad \psi_2(\boldsymbol{r}) = \frac{1}{\sqrt{\pi}} e^{-|\boldsymbol{r}-\boldsymbol{R}|}\,, \tag{4.4}$$

for electrons moving around the left/right nuclear charge respectively.

The density of a two electron system is calculated as

$$n(\boldsymbol{r}) = \int d\boldsymbol{r}_2\, |\Psi_{\text{elec}}(\boldsymbol{r}, \boldsymbol{r}_2)|^2\,. \tag{4.5}$$

The integral obtained from this formula with wave functions as in Equation 4.4 is solvable and gives

$$n(\boldsymbol{r}) = \frac{1}{\pi}\left(e^{-2|\boldsymbol{r}|} + e^{-2|\boldsymbol{r}-\boldsymbol{R}|} - 2e^{-(|\boldsymbol{r}|+|\boldsymbol{r}-\boldsymbol{R}|)} e^{-R}\left(1 + R + \frac{R^2}{3}\right)\right)\,, \tag{4.6}$$

where $R = |\boldsymbol{R}|$.

The first two terms are the addition of the two atomic densities while the exponentially smaller last term is coming from the fermionic nature of the two-electron wave function in Equation 4.3. The Pauli exclusion principle present in a fermionic system acts as a repulsive force between the electrons and lowers the electron density between atoms. It is, however, also evident that if R is large we can neglect this density lowering and the *overlap* term:

$$\int d\boldsymbol{r}\, \psi_1(\boldsymbol{r})\psi_2(\boldsymbol{r}) \approx 0\,. \tag{4.7}$$

The perturbation

The first thing to decide in perturbation theory is what the perturbation is. In our case there are two competing views. One is derived from how the ion at $\boldsymbol{R}$ affects the single electron hydrogen like system at the origin. As seen in Figure 4.1 adding the two hydrogen potentials substantially lowers the potential barrier between the two ions. This means that high kinetic energy electrons can venture somewhat further towards the other ion. The other view is that the other system, combined of an equal amount of positive charge from the ion and negative charge from the electrons, is charge neutral and that this screened potential

does not affect the potential barrier very much, so that the important perturbation instead is the coulomb potential between the two electrons. It was not evident to the authors of this report which view to take, so we examined both.

The strategy in the first case is to do a stepwise perturbation theory. First we see how the bare ionic potential at $\boldsymbol{R}$ affects the wave functions of the single electron around the ion at the origin. Then we use these perturbed single electron wave functions in a two body wave function according to Equation 4.3 and calculate the effect of the coulomb potential between the two electrons. If the unperturbed single electron hamiltonian for the hydrogen system at the origin is denoted H_1 we have:

$$1) \qquad H_{A1} = H_1 - \frac{1}{|\boldsymbol{r}_1 - \boldsymbol{R}|} + \frac{1}{R} \tag{4.8}$$

$$2) \qquad H = H_{A1} + H_{A2} + \frac{1}{|\boldsymbol{r}_1 - \boldsymbol{r}_2|} - \frac{1}{R}\,,. \tag{4.9}$$

where factors of $1/R$ from the ion-ion interaction, retain charge neutrality, in each step taking away the leading, in the end vanishing, term.

In the other case we have the two electron hamiltonian:

$$H = H_1 + H_2 - \frac{1}{|\boldsymbol{r}_1 - \boldsymbol{R}|} - \frac{1}{|\boldsymbol{r}_2|} + \frac{1}{|\boldsymbol{r}_1 - \boldsymbol{r}_2|} + \frac{1}{R}\,, \tag{4.10}$$

where the unperturbed two electron wave functions are derived from H_1 and H_2.

First order perturbation theory

We will now simplify the notations in order to make the following discussion more transparent. We will denote a single particle wave function with $|\ >$. So that the single particle hydrogen like wave function in Equation 4.1 reads

$$\psi_{nLM}(\boldsymbol{r}) \text{ centered on atom } 1 = |nL; 1; \boldsymbol{r} >\,, \tag{4.11}$$

where we have omitted the index M since it will never enter into our discussion because we chose the z-axis of our system to be along the $\boldsymbol{R}$ vector. The wave functions in Equation 4.4 are thus denoted $|1s; 1; \boldsymbol{r} >$ and $|1s; 2; \boldsymbol{r} >$, respectively.

The integral we solved to arrive at the zero order density for the two hydrogen system in Equation 4.6 looks like

$$|1; 2; \boldsymbol{r}; \boldsymbol{r}_2 > \;=\; |1s; 1; \boldsymbol{r} > |1s; 2; \boldsymbol{r}_2 > - |1s; 2; \boldsymbol{r} > |1s; 1; \boldsymbol{r}_2 > \tag{4.12}$$

$$n(\boldsymbol{r}) \;=\; < 1; 2; \boldsymbol{r}; \boldsymbol{r}_2 | 1; 2; \boldsymbol{r}; \boldsymbol{r}_2 > \;. \tag{4.13}$$

We also note that $< 1s; 1; \boldsymbol{r} | 1s; 1; \boldsymbol{r} >= 1$ and that the overlap $< 1s; 1; \boldsymbol{r} | 1s; 2; \boldsymbol{r} >= 0$.

Energy

In first order perturbation theory, the first order correction to the energy is $< |\text{perturbation}| >$, which in our case leads to numerous solvable integrals of the type

$$< 1s; 1; \boldsymbol{r}_2 | \frac{1}{|\boldsymbol{r} - \boldsymbol{r}_2|} | 1s; 1; \boldsymbol{r}_2 > = \frac{1}{r} \left(1 - e^{-2r} (1 + r) \right) , \tag{4.14}$$

where $r = |\boldsymbol{r}|$. Using this and neglecting exponentially small terms similarly to ignoring the overlap, we for the electron-ion interaction terms obtain

$$< 1s; 2; \boldsymbol{r}_2 | \frac{1}{|\boldsymbol{r}_2|} | 1s; 2; \boldsymbol{r}_2 > = < 1s; 1; \boldsymbol{r}_1 | \frac{1}{|\boldsymbol{R} - \boldsymbol{r}_1|} | 1s; 1; \boldsymbol{r}_1 > \quad \approx \quad \frac{1}{R} \tag{4.15}$$

$$\tag{4.16}$$

and these terms will cancel with the charge neutrality terms that we introduced above.

The electron-electron coulomb repulsion terms in the two-electron picture needs a little more work:

$$< 1s; 2; \boldsymbol{r}_1 | \; < 1s; 1; \boldsymbol{r}_2 | \frac{1}{|\boldsymbol{r}_1 - \boldsymbol{r}_2|} | 1s; 1; \boldsymbol{r}_2 > \; | 1s; 2; \boldsymbol{r}_1 > = \tag{4.17}$$

$$< 1s; 2; \boldsymbol{r}_1 | \frac{1}{|\boldsymbol{r}_1|} \left(1 - e^{-2|\boldsymbol{r}_1|} (1 + |\boldsymbol{r}_1|) \right) | 1s; 2; \boldsymbol{r}_1 > = \tag{4.18}$$

$$\approx \frac{1}{R} - \frac{1}{\pi} \int d\boldsymbol{r_1} \frac{e^{-2|\boldsymbol{r}_1 - \boldsymbol{R}|} \, e^{-2|\boldsymbol{r}_1|} (1 + |\boldsymbol{r}_1|)}{|\boldsymbol{r}_1|} \approx \frac{1}{R} , \tag{4.19}$$

again canceling with the charge neutrality term.

It is clear that the first order energy contribution is zero in both the schemes we are investigating.

Wave functions

While the first order energy contribution is zero, the first order wave function changes are needed for the next step in the first scheme.

The first order correction to the single electron wave function on atom 1 are

$$\sum_{nL \neq 1s} \frac{< 1s; 1; \boldsymbol{r} | - \frac{1}{|\boldsymbol{r} - \boldsymbol{R}|} + \frac{1}{R} | nL; 1; \boldsymbol{r} >}{E_n - E_1} | nL; 1; \boldsymbol{r} > = \sum_{nL \neq 1s} c_{nL} | nL; 1; \boldsymbol{r} > \; . \tag{4.20}$$

Note that $< 1s; 1; \boldsymbol{r} | nL; 1; \boldsymbol{r} > = 0$; the eigenstates of the unperturbed hamiltonian are orthogonal, so the second term in the perturbation potential, the charge neutrality term, is not contributing to c_{nL}.

The integrals to solve for obtaining a general formula for c_{nL} are non-trivial. A good approximation for c_{nL}, valid for $n/2R << 1$, is

$$c_{nL} = \left(\frac{n}{2R}\right)^{L+1} \left[\frac{(n+L)!}{(n-L-1)!}\frac{1}{2L+1}\right]^{\frac{1}{2}} \left(\frac{4}{n^2-1}\right)^{L+3} L\, n^3 \left(\frac{n-1}{n+1}\right)^n \frac{1}{4}\,. \tag{4.21}$$

Note that the singularity at $n = 1$ is fictitious since the $1s$ state should be excluded in the sum in Equation 4.20 and it is the only allowed state for $n = 1$. Also note that this $1s$ wave function perturbation has no s components since $c_{n0} = 0$. A formula for larger n has also been derived, but since it is not vital for the discussion in this report, we omit it.

For the second step in the first scheme we now use the perturbed single electron wave functions,

$$|1s;1;\boldsymbol{r}>_p = |1s;1;\boldsymbol{r}> + \sum_{nL\neq 1s} c_{nL}|nL;1;\boldsymbol{r}>\,, \tag{4.22}$$

in the two electron wave function in Equation 4.3, and calculate the energy from the hamiltonian in Equation 4.9. We should also note that the overlap calculated with this perturbed wave function still is exponetially small, ${}_p< 1s;1;\boldsymbol{r}|1s;2;\boldsymbol{r}>_p = 0$.

$$\begin{aligned}
&2({}_p< 1s;1;\boldsymbol{r}_1|1s;1;\boldsymbol{r}_1>_p)^2 E_{\text{tot}} = \\
&\quad = ({}_p< 1s;1;\boldsymbol{r}_1|\,{}_p< 1s;2;\boldsymbol{r}_2| - {}_p< 1s;2;\boldsymbol{r}_1|\,{}_p< 1s;1;\boldsymbol{r}_2|) \times \\
&\qquad H(\boldsymbol{r}_1,\boldsymbol{r}_2)\,(|1s;1;\boldsymbol{r}_1>_p|1s;2;\boldsymbol{r}_2>_p - |1s;2;\boldsymbol{r}_1>_p|1s;1;\boldsymbol{r}_2>_p) \qquad (4.23)\\
&\quad = {}_p< 1s;1;\boldsymbol{r}_1|\,{}_p< 1s;2;\boldsymbol{r}_2|H(\boldsymbol{r}_1,\boldsymbol{r}_2)|1s;1;\boldsymbol{r}_1>_p|1s;2;\boldsymbol{r}_2>_p \\
&\qquad + {}_p< 1s;2;\boldsymbol{r}_1|\,{}_p< 1s;1;\boldsymbol{r}_2|H(\boldsymbol{r}_1,\boldsymbol{r}_2)|1s;2;\boldsymbol{r}_1>_p|1s;1;\boldsymbol{r}_2>_p \\
&\qquad - {}_p< 1s;1;\boldsymbol{r}_1|\,{}_p< 1s;2;\boldsymbol{r}_2|H(\boldsymbol{r}_1,\boldsymbol{r}_2)|1s;2;\boldsymbol{r}_1>_p|1s;1;\boldsymbol{r}_2>_p \\
&\qquad - {}_p< 1s;2;\boldsymbol{r}_1|\,{}_p< 1s;1;\boldsymbol{r}_2|H(\boldsymbol{r}_1,\boldsymbol{r}_2)|1s;1;\boldsymbol{r}_1>_p|1s;2;\boldsymbol{r}_2>_p \qquad (4.24)\\
&\quad = {}_p< 1s;2;\boldsymbol{r}_2|1s;2;\boldsymbol{r}_2>_p\ {}_p< 1s;1;\boldsymbol{r}_1|H_{A1}|1s;1;\boldsymbol{r}_1>_p \\
&\qquad + {}_p< 1s;1;\boldsymbol{r}_1|1s;1;\boldsymbol{r}_1>_p\ {}_p< 1s;2;\boldsymbol{r}_2|H_{A2}|1s;2;\boldsymbol{r}_2>_p + \\
&\qquad + {}_p< 1s;1;\boldsymbol{r}_1|\,{}_p< 1s;2;\boldsymbol{r}_2|\frac{1}{|\boldsymbol{r}_1-\boldsymbol{r}_2|} - \frac{1}{R}|1s;1;\boldsymbol{r}_1>_p|1s;2;\boldsymbol{r}_2>_p \\
&\qquad + {}_p< 1s;1;\boldsymbol{r}_2|1s;1;\boldsymbol{r}_2>_p\ {}_p< 1s;2;\boldsymbol{r}_1|H_{A1}|1s;2;\boldsymbol{r}_1>_p \\
&\qquad + {}_p< 1s;2;\boldsymbol{r}_1|1s;2;\boldsymbol{r}_1>_p\ {}_p< 1s;1;\boldsymbol{r}_2|H_{A2}|1s;1;\boldsymbol{r}_2>_p + \\
&\qquad + {}_p< 1s;2;\boldsymbol{r}_1|\,{}_p< 1s;1;\boldsymbol{r}_2|\frac{1}{|\boldsymbol{r}_1-\boldsymbol{r}_2|} - \frac{1}{R}|1s;2;\boldsymbol{r}_1>_p|1s;1;\boldsymbol{r}_2>_p \\
&\qquad - 2\,{}_p< 1s;1;\boldsymbol{r}_1|\,{}_p< 1s;2;\boldsymbol{r}_2|\frac{1}{|\boldsymbol{r}_1-\boldsymbol{r}_2|}|1s;2;\boldsymbol{r}_1>_p|1s;1;\boldsymbol{r}_2>_p \\
&\qquad - 2\,{}_p< 1s;2;\boldsymbol{r}_1|\,{}_p< 1s;1;\boldsymbol{r}_2|\frac{1}{|\boldsymbol{r}_1-\boldsymbol{r}_2|}|1s;1;\boldsymbol{r}_1>_p|1s;2;\boldsymbol{r}_2>_p\,, \qquad (4.25)
\end{aligned}$$

where we have neglected terms involving the exponentially small overlap. By symmetry we can deduce that all H_A terms give the same contribution. The last two terms, the electron-

electron interaction overlap integrals, can be show to be exponentially small already for the pure $1s$ state.

We know from above that terms only containing $1s$ states will only contribute the non-perturbed sum of energies from the two individual hydrogen systems. By explicitly solving the integrals for the perturbed wave function with largest coefficient, the $2p_z$ state

$$|2p_z; 1; \boldsymbol{r} >= \frac{1}{4\sqrt{2\pi}} e^{-\frac{r}{2}} r\cos(\theta)\,, \tag{4.26}$$

($n = 2$, $L = 1$, and $M = 0$), and also noting that states with $M \neq 0$, such as $2p_x$ and $2p_y$ will not contribute to the perturbed wave function due to the symmetry of the perturbation, we conclude that all terms involving only one such state also cancel. When solving these integrals it is useful to note that they are similar to the integral for the coefficient c_{nL} in Equation 4.20.

Thus it only remains to evaluate the terms that involve two $2p_z$ states.

$$\begin{aligned} 2(1+c_{2p}^2)^2 E_{\text{tot}} &= 4E_1(1+c_{2p}^2)^2 + (c_{2p})^2 \Bigg(4 < 2p_z; 1; \boldsymbol{r}_1| \frac{-1}{|\boldsymbol{r}_1 - \boldsymbol{R}|} |2p_z; 1; \boldsymbol{r}_1 > + \\ & 4 < 2p_z; 2; \boldsymbol{r}_1| < 1s; 1; \boldsymbol{r}_2| \frac{1}{|\boldsymbol{r}_1 - \boldsymbol{r}_2|} - \frac{1}{R} |1s; 1; \boldsymbol{r}_2 > |2p_z; 2; \boldsymbol{r}_1 > + \\ & 8 < 2p_z; 2; \boldsymbol{r}_1| < 1s; 1; \boldsymbol{r}_2| \frac{1}{|\boldsymbol{r}_1 - \boldsymbol{r}_2|} - \frac{1}{R} |2p_z; 1; \boldsymbol{r}_2 > |1s; 2; \boldsymbol{r}_1 > \Bigg) . \end{aligned} \tag{4.27}$$

It is evident that the two first integrals cancel. Thus we are left with a term coupling the p character of the electron on one atom with the s character of the one on the other atom, via the electron-electron interaction:

$$< 1s; 2; \boldsymbol{r}_1| < 1s; 1; \boldsymbol{r}_2| \frac{1}{|\boldsymbol{r}_1 - \boldsymbol{r}_2|} |2p_z; 1; \boldsymbol{r}_2 > |2p_z; 2; \boldsymbol{r}_1 > \ . \tag{4.28}$$

We should note that I have used the $2p$ state here only to simplify the discussion. The common view adopts this picture and thus discusses van der Waals' interactions in terms of *dipoles*. However, the perturbation of a spherically symmetric electron density distribution due to a distant atom also introduces higher order state character into the wave functions and thus also higher multipoles.

While this two step perturbation theory view gives us insight into the mechanisms of the van der Waals' interaction, the uneven treatment of perturbations of equal size, the electron-ion to second order while the electron-electron only is first order, also complicates the book keeping and as we will see, gives of the wrong asymptotic behavior. In the next section we will thus treat all perturbations as one single perturbative potential, following the second scheme of second order perturbation theory.

Second order perturbation theory

We have already shown that the first order perturbation theory contribution to the energy of the two electron system is zero. The second order energy contribution is

$$E^{(2)} = \sum_{\substack{nL,n'L' \text{not} \\ \text{both } 1s}} \frac{\left| < 1s;1;\boldsymbol{r}_1| < 1s;2;\boldsymbol{r}_2| - \frac{1}{|\boldsymbol{r}_1-\boldsymbol{R}|} - \frac{1}{|\boldsymbol{r}_2|} + \frac{1}{|\boldsymbol{r}_1-\boldsymbol{r}_2|} + \frac{1}{R}|nL;1;\boldsymbol{r}_1 > |n'L';2;\boldsymbol{r}_2 > \right|^2}{2E_1 - E_n - E_{n'}} . \tag{4.29}$$

The essential difference from the two-step scheme is that the electron-electron interaction, the $1/|\boldsymbol{r}_1 - \boldsymbol{r}_2|$ term, is included in the perturbation of the wave functions at first order while the two-step perturbation of the wave function only includes the ion-electron interactions.

In Figure 4.2 we see that the states on the atoms are well localized around each individual atom as long as $\boldsymbol{R}$ is large. The wave functions will thus naturally limit the integration

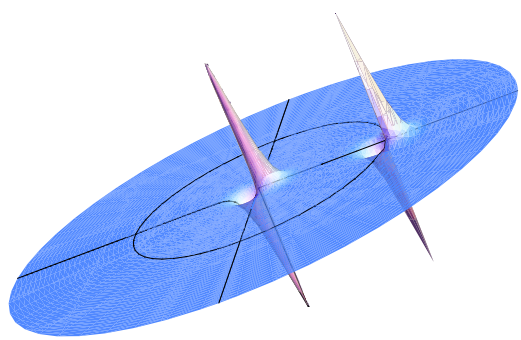

Figure 4.2. The states, here illustrated by the $2p_z$ states, on each atom, are well localized and do not overlap.

regions to small regions around each atom. Mathematically, if we have $\boldsymbol{r}_1$ and $\boldsymbol{r}_2$ as electron coordinate on the 1 and 2 atom respectively, $\boldsymbol{r}_1$ and $\boldsymbol{r}_2 - \boldsymbol{R}$ will be small compared to $\boldsymbol{R}$. We can expand the potential terms in Equation 4.29 using

$$\frac{1}{|\boldsymbol{R}-\boldsymbol{x}|} = \frac{1}{R}\frac{1}{\sqrt{1 - 2\frac{\boldsymbol{x}\cdot\hat{\boldsymbol{R}}}{R} + \frac{\boldsymbol{x}\cdot\boldsymbol{x}}{R^2}}} = \frac{1}{R}\left(1 + \frac{\boldsymbol{x}\cdot\hat{\boldsymbol{R}}}{R} + \frac{\frac{3}{8}(2\boldsymbol{x}\cdot\hat{\boldsymbol{R}})^2 - \frac{1}{2}\boldsymbol{x}\cdot\boldsymbol{x}}{R^2}\right) , \tag{4.30}$$

where $\hat{\boldsymbol{R}}$ is a unit vector in the $\boldsymbol{R}$ direction and the magnitude of $\boldsymbol{x}$ is small. We note that $\boldsymbol{r}_1 - \boldsymbol{r}_2 = -\boldsymbol{R} + \boldsymbol{r}_1 + (\boldsymbol{R} - \boldsymbol{r}_2)$ with the sum of the last two terms small compared to the first $-\boldsymbol{R}$ term. Straightforward bookkeeping shows that all terms proportional to $1/R^2$, from the

second term on the right hand side in Equation 4.30, cancel. This is completely analogous to all the terms canceling in the two step scheme to eliminate the first order perturbation. There are cancellations also between the $1/R^3$ terms, analogous to the one in Equation 4.27, and only terms with products of the small variables $\boldsymbol{r}_1$ and $\boldsymbol{r}_2 - \boldsymbol{R}$ remains. We arrive at

$$-\frac{1}{|\boldsymbol{r}_1 - \boldsymbol{R}|} - \frac{1}{|\boldsymbol{r}_2|} + \frac{1}{|\boldsymbol{r}_1 - \boldsymbol{r}_2|} + \frac{1}{R} \approx \frac{-1}{R^3}\left(3\left(\boldsymbol{r}_1 \cdot \hat{\boldsymbol{R}}\right)\left([\boldsymbol{r}_2 - \boldsymbol{R})\right] \cdot \hat{\boldsymbol{R}}\right) - \boldsymbol{r}_1 \cdot (\boldsymbol{r}_2 - \boldsymbol{R})\right) . \quad (4.31)$$

The symmetry of this perturbation potential implies that only states with p symmetry in both $\boldsymbol{r}_1$ and $\boldsymbol{r}_2$ will contribute to the sum in Equation 4.29. Thus, again, we arrive to the conclusion that we need at least 2 p-states in integrals like in Equation 4.28. However, in the two-step perturbation theory scheme only the $2p_z$ state contributed while the second term in Equation 4.31 also will be non-zero for $2p_x$ and $2p_y$ states. This again shows the un-eveness in the treatment of small perturbations in the two-step scheme. Note that if we had retained more terms in the expansion in 4.30, we would have obtained contributions also from d, f and higher states, however with an increasing number of factors of $1/R$.

Performing the integrals in Equation 4.29 we arrive at

$$E^{(2)} \propto -\frac{1}{R^6} . \quad (4.32)$$

Note that the minus sign is coming from the energy difference term in the nominator which will always be negative, irrespectively of nL. The interaction between the two systems lowers the energy compared to the separate systems; the van der Waals' force is *attractive*.

Returning briefly to the two step perturbation scheme, we note that the terms as in Equation 4.28 will contribute $(c_{2p})^2/R^3 = 1/R^7$ to the energy. Again this erroneous result being due to the electron-electron interaction not being included in the perturbing potential in the first step.

Summary

As seen from the discussion and derivations above, the van der Waals' forces arise from a intricate synchronization between states on two nearby, but separate, systems. By separate we here mean that electrons are very unlikely to actively hop from one atom to another, so called tunneling. This picture is also supported by the overlap integrals remaining exponentially small even in the perturbed states.

The common picture is that of *fluctuating dipoles*: Electrons in one system spontaneously displace themselves by excitations into non-spherical states (p states) to create a dipole, which the electrons in the other system respond to, setting up a dipole field in their turn. This picture, however, implies a time dependence and a non-equilibrium situation that might not be the correct picture.

From a DFT perspective this strongly suggests *non-locality*. However, the second order perturbation picture leads us to consider another picture, based on the close connection

between *effective potential* and *density*. It is possible that the electrons/density in one system modifies the effective potential, which contains all many-body interactions in DFT and is *local*, in a way that influences the electron density in the other system. It is not evident, however, how such a mechanism would be established, and for the time being it remains a conjecture.

Chapter 5

Density Functional Theory exchange-correlation functionals

As explained in the Introduction in Chapter 1, all many-body interactions present in a real system can be expressed as an *exchange-correlation functional* acting on densities composed from single particle orbitals in the Kohn-Sham picture. There are two main lines of thought concerning including van der Waals' forces in an exchange-correlation functional. One is based on the $1/R^6$ behavior demonstrated above, and one is based on the non-locality concept.

$1/R^6$ functionals

This group of functionals is mainly concerned with obtaining a good approximation for the coefficient of the $1/R^6$ term. This coefficient is the polarizability of an atom. If an atom is in a environment with other electrons, the bare atomic polarizability will be modified. Another crucial ingredient in this type of functionals is the "damping function"; since the $1/R^6$ term diverges as $R \to 0$ a function that seamlessly join this attractive term to the ordinary repulsion at closer distances is needed. As is seen in Figure 5.1, the equilibrium binding distance is fully set by the damping function, and for our purpose of understanding molecular crystals at equilibrium, the poor knowledge about how a proper damping function should look like makes this approach less interesting.

While this approach is widely used since it is quite easy to tune coefficients and damping functions to provide decent results for specific materials, the resulting vdWs' functionals only work for limited sets of systems. As so often is the case in the functional developing business, the large number of vdWs' functionals show how important it is to include vdWs' forces for many applications, but also that none of them is generally applicable (if so, everyone needing a vdWs' functional would use this generally applicable one).

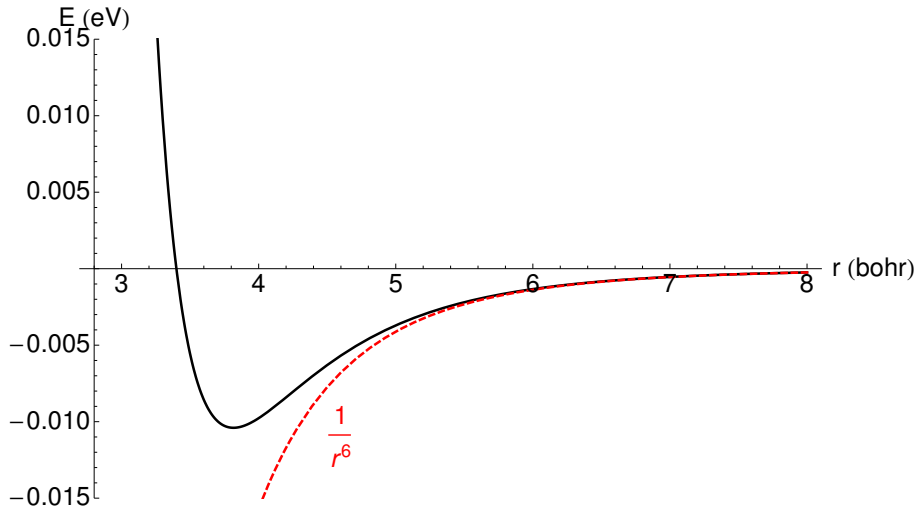

Figure 5.1. A Lennard-Jones 6-12 potential approximately describing the the binding energy of two Ar atoms at distance r. As is seen, the $1/r^6$ term diverges as the distance between the atoms is decreasing and a damping term is needed to turn the potential upwards for correct binding profile.

Non-local functionals

The other line of development has resulted in a few functionals, mainly designed by the groups of Langreth and Lundqvist at Rutgers University and Chalmers University of Technology, Sweden, respectively. While this approach is more rigorous than the one described above, it has been plagued by a disconnect between the derivation of the van der Waals' terms, and the derivation of the underlying functional describing binding energies at closer distances, analogous to the damping function. In the last few years Ann Mattsson has set up collaborations with herself, Rickard Armiento at Linköping University, Sweden, and Torbjörn Björkman at Alvar Aalto University, Espoo, Finland to explore fundamental questions in this area. However, the work is progressing slowly since both are doing their main research efforts in other areas.

Chapter 6

Summary and Conclusion

Despite the lack of proper van der Waals' treatment, we were successful at using DFT-MD to predict the unreacted Hugoniots of PETN and HNS. Under compression, errors in the attractive crystal forces appear to be negligible as we obtained excellent results. This method provides all of the necessary information to build a complete equation of state, but validation of predicted temperatures is still needed. Our ultimate goal is to create a tabular equation of state for use in hydrocode simulations. We are also pursuing research that will result in a new exchange-correlation functional that will accurately describe van der Waals' forces and the equilibrium bonding of molecular crystal explosives.

The origins of van der Waals' forces are an intricate collective of effects due to the interaction between electrons on one atom and the electrons and ion forming another, distant, atom. It results in an weak attractive force between the atoms. While it is important to consider this origin and mechanism when developing new exchange-correlation functionals for use in DFT, this cannot be the sole focus since the equilibrium distance, for example, is determined by how the atoms interact at smaller distances. A proper functional needs to seamlessly be able to include the van der Waals' forces at large distances while still retaining the good description of matter under compression currently available in, for example, AM05. The construction of a generally adequate functional incorporating van der Waals' forces is still an elusive goal and future efforts from our team will be focused on the duality of the electron *density* and the <u>local</u> *effective potential*.

References

[1] R. Armiento and A. E. Mattsson. Functional designed to include surface effects in self-consistent density functional theory. *Phys. Rev. B*, 72:085108, Aug 2005.

[2] E. F. C. Byrd and B Rice. Ab initio study of compressed 1,3,5,7-tetranitro-1,3,5,7-tetraazacyclooctane (hmx), cyclotrimethylenetrinitramine (rdx), 2,4,6,8,10,12-hexanitrohexaazaisowurzitane (cl-20), 2,4,6-trinitro-1,3,5-benzenetriamine (tatb), and pentaerythritol tetranitrate (petn). *J. Phys. Chem. C*, 111:2787, 2007.

[3] Michael Carroll and Albert C. Holt. Suggested modification of the p-alpha model for porous materials. *J. Appl. Phys.*, 43:759, 1971.

[4] J. W. Conant, H. H. Cady, R. R. Ryan, J. L. Yarnell, and J. M. Newsam. The atom positions of pentaerythritol tetranitrate (petn, c5h8n4o12) determined by x-ray and by neutron diffraction. Technical report LA-7756- MS, Los Alamos Scientific Laboratory, 1979.

[5] John O. Erkman and David J. Edwards. Computed and experimental hugoniots for unreacted porous explosives. In D. J. Edwards and S. J. Jacobs, editors, *Sixth International Detonation Symposium*, pages 766–776, Arlington, VA, 1976. Office of Naval Research.

[6] Par Francios Gerard and Antione Hardy. Structure de l'hexanitro-2,2"4,4"6,6' stilbene, hns, et comparaison avec le trinitro-2,4,6 tolu6ne, tnt. *Acta Cryst.*, C44:1283–1287, 1988.

[7] W. Herrmann. Constitutive equation for the dynamic compaction of ductile porous materials. *J. Appl. Phys.*, 40:2490, 1969.

[8] P. Hohenberg and W. Kohn. Inhomogeneous electron gas. *Phys. Rev.*, 136:B864–B871, Nov 1964.

[9] M. D. Knudson and M. P. Desjarlais. Shock compression of quartz to 1.6 tpa: Redefining a pressure standard. *Phys. Rev. Lett.*, 103:225501, Nov 2009.

[10] W. Kohn and L. J. Sham. Self-consistent equations including exchange and correlation effects. *Phys. Rev.*, 140:A1133–A1138, Nov 1965.

[11] G. Kresse and J. Furthmüller. Efficient iterative schemes for *ab initio* total-energy calculations using a plane-wave basis set. *Phys. Rev. B*, 54:11169–11186, Oct 1996.

[12] G. Kresse and J. Hafner. *Ab initio* molecular dynamics for liquid metals. *Phys. Rev. B*, 47:558–561, Jan 1993.

[13] G. Kresse and J. Hafner. *Ab initio* molecular-dynamics simulation of the liquid-metal amorphous-semiconductor transition in germanium. *Phys. Rev. B*, 49:14251–14269, May 1994.

[14] G. Kresse and D. Joubert. From ultrasoft pseudopotentials to the projector augmented-wave method. *Phys. Rev. B*, 59:1758–1775, Jan 1999.

[15] Rudolph J. Magyar, Ann E. Mattsson, and Peter A. Schultz. Some practical considerations for density functional theory studies of chemistry at metal surfaces. In Thomas C. Allison, Orkid Coskuner, and Carlos A. González, editors, *Metallic Systems: A Quantum Chemist's Perspective*. CRC Press, Boca Raton, London, New York, 2011.

[16] S. P. March, editor. *LASL Shock Hugoniot Handbook*, Berkeley, CA, 1980. University of California Press.

[17] Ann E. Mattsson. In pursuit of the "divine" functional. *Science*, 298(5594):759–760, 2002.

[18] Ann E. Mattsson, Rickard Armiento, Joachim Paier, Georg Kresse, John M. Wills, and Thomas R. Mattsson. The AM05 density functional applied to solids. *Journal of Chemical Physics*, 128(8):084714, 2008.

[19] Ann E Mattsson, Peter A Schultz, Michael P Desjarlais, Thomas R Mattsson, and Kevin Leung. Designing meaningful density functional theory calculations in materials science: a primer. *Modelling and Simulation in Materials Science and Engineering*, 13(1):R1, 2005.

[20] Ann E. Mattsson, Ryan R. Wixom, and Thomas R. Mattsson. Calculating hugoniots for molecular crystals from first principles. In C. B. S. Peiris and B. Asay, editors, *Fourteenth International Detonation Symposium*, ONR 351-10-185, page 1043, Arlington, VA, 2010. Office of Naval Research.

[21] Seth Root, Rudolph J. Magyar, John H. Carpenter, David L. Hanson, and Thomas R. Mattsson. Shock compression of a fifth period element: Liquid xenon to 840 GPa. *Phys. Rev. Lett.*, 105:085501, Aug 2010.

[22] G. E. Seay and L. B. Seely. Initiation of a low?density petn pressing by a plane shock wave. *J. Appl. Phys.*, 32:1092, 1961.

[23] Dante Stirpe, James O. Johnson, and Jerry Wackerle. Shock initiation of xtx-8003 and pressed petn. *J. Appl. Phys.*, 41:3884, 1970.

[24] Ya. B. Zel'dovich and Yu. P. Raizer. *Physics of Shock Waves and High-Temperature Hydrodynamic Phenomena*. Dover Publications, 2002.

DISTRIBUTION:

1	MS 1189	Thomas R. Mattsson, 01641 (electronic copy)
1	MS 1318	Bruce A. Hendrickson, 01440 (electronic copy)
1	MS 1322	Ann E. Mattsson, 01443 (electronic copy)
1	MS 1323	Erik O. Strack, 01443 (electronic copy)
1	MS 1454	Leanna Minier, 02554 (electronic copy)
1	MS 1454	David L Damm, 02554 (electronic copy)
1	MS 1454	Ryan R. Wixom, 02554 (electronic copy)
1	MS 0899	Technical Library, 9536 (electronic copy)

Sandia National Laboratories